Inorg. Chem. **2009**, *48*, 1323−1333

Theoretical Study of the Oxidation Reaction and Electron Spin Resonance Parameters Involving Sulfite Oxidase

Elizabeth Hernandez-Marin and Tom Ziegler*

Department of Chemistry, University of Calgary, 2500 University Drive NW, Calgary, Alberta, Canada T2N 1N4

Received June 23, 2008

We present a density functional theory (DFT) study on the conversion of sulfite to sulfate with a model complex representing the active site of the molybdenum-containing enzyme sulfite oxidase (SO). This study considers the attack of the sulfur lone pair from SO_3^{2-} on the equatorial oxo ligand of the model complex as the initial step in the oxidation process. The good agreement between our energy profile and data derived from experimental kinetic parameters provides some support for the reaction mechanism of the oxidative half-reaction of SO proposed in this study. The enzymatic reductive half-reaction involves the formation of an Electron Spin Resonance (ESR) active Mo(V) species. Experimentally, differences in ESR parameters (g-values and ^{1}H hyperfine coupling constant) of the low- and high-pH forms of the enzyme have been found. The current study also presents DFT-based calculations on ESR parameters for three model complexes representing the paramagnetic center Mo(V) of SO in its possible low- and high-pH forms. We provide an analysis of the magnetic orbital coupling responsible for the calculated g-values. Finally, we suggest how the conformation and hydrogen bonding interactions of the hydroxyl ligand can explain the different ESR parameters at low- and high-pH.

1. Introduction

Molybdenum is present at the active sites of metalloenzymes that execute key transformations in the metabolism of nitrogen, sulfur, carbon, arsenic, selenium, and chlorine compounds.[1] It is widely available to biological systems because of the solubility of its high-valent oxides in water. With the exception of the molybdenum center in nitrogenases, the molybdenum cofactors have been identified as molybdenum-pterin complexes (Figure 1). The Mo center in these complexes couples electron-transfer to atom-transfer chemistry.[2] In particular it catalytically transfers an oxygen atom either to or from a physiological acceptor/donor molecule.[1] Examples are the reduction of nitrate to nitrite, dimethyl sulfoxide to dimethyl sulfide, and the oxidation of sulfite to sulfate. In recent years, progress has been made in the study of molybdenum-containing enzymes from a variety of organisms.[1,3,4]

The majority of molybdoenzymes can be classified into three families (Supporting Information, Figure S1) represented by xanthine oxidase (XO), sulfite oxidase (SO), and DMSO reductase.[5] Sulfite oxidase catalyzes the physiologically vital oxidation of sulfite to sulfate, the terminal reaction in the oxidative degradation of the sulfur-containing amino acids cysteine and methionine.[1] In this enzyme, molybdenum is coordinated by five ligands with an approximately square pyramidal coordination geometry. The equatorial plane is occupied by three sulfur ligands and one water/hydroxo ligand whereas an oxo group occupies the axial position.

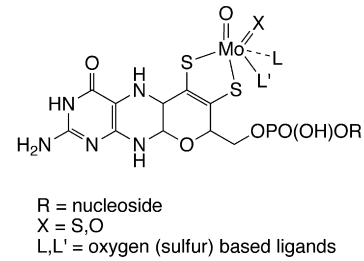

Figure 1. Pterin cofactor.

* To whom correspondence should be addressed. E-mail: ziegler@ucalgary.ca.

(1) Hille, R. *Chem. Rev.* **1996**, *96*, 2757.
(2) Cowan, J. A. *Inorganic Biochemistry. An introduction*; Wiley-VCH: New York, 1997; p 214.
(3) Hille, R. *Trends Biochem. Sci.* **2002**, *27*, 360.
(4) Feng, C.; Tollin, G.; Enemark, J. H. *Biochim. Biophys. Acta* **2007**, *1774*, 527.
(5) Basu, P.; Stolz, J. F.; Smith, M. T. *Curr. Sci.* **2003**, *84*, 1412.

10.1021/ic801158t CCC: $40.75
Published on Web 01/13/2009

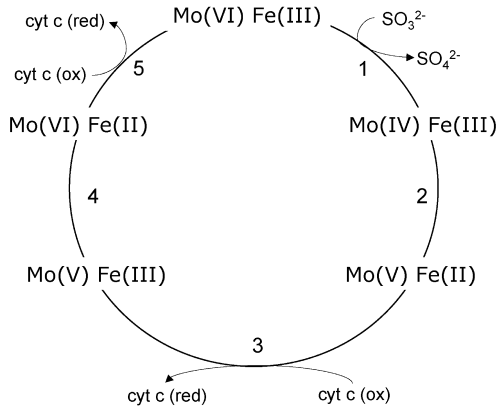

Figure 2. Accepted reaction cycle of the molybdenum-containing enzyme sulfite oxidase.

According to the postulated mechanism for sulfite oxidase,[6] in the reductive half-cycle the sulfate is released and an oxygen-containing ligand from the solvent is then coordinated to the Mo(IV) center (step 1, Figure 2). The oxidative half-cycle consists of two one-electron intramolecular transfers to obtain first Mo(V) and then Mo(VI) (steps 2 and 4, Figure 2) and two one-electron transfers from the heme Fe(II) to the terminal electron aceptor, cytochrome c (ox) (steps 3 and 5, Figure 2).

Different studies on model systems[7,8] and purified enzyme[6,9,10] have established a mechanism consistent with Michaelis−Menten kinetics. In this mechanism it is suggested that the SO_3^{2-} oxidation takes place by an attack of a sulfur lone pair on the equatorial oxo group coordinated to the Mo (VI) center.[6,7]

The five-coordinated distorted square pyramidal geometry of the metal center of SO has been established by X-ray crystallography.[11−13] Electron Spin Resonance (ESR) studies on the Mo(V) species have shown that at pH = 7 the equatorial ligand is a hydroxyl group while at pH = 9.5 the oxygen-containing ligand in the equatorial plane could be either OH^- or H_2O.[14−16]

Density Functional Theory (DFT) methods provide an excellent complementary tool to experimental techniques and have been used, mostly based on synthetic analogues, to model the reaction mechanisms of molybdoenzymes such as DMSO reductase[17,18] and XO.[19−22] Particularly in the case of SO, a combined EXAFS and DFT study has suggested that the equatorial O-donor in the reduced form of the enzyme, Mo (VI), is most likely water.[23] The sulfite oxidation step in Figure 2 has been modeled by considering the reaction of the six-coordinated synthetic analogue complex $[MoO_2(mnt)_2]^{2-}$ with HSO_3^-. The study considered the attack of the sulfur lone pair on one of the oxo-groups.[24] In the actual enzyme, the molybdenum center is a five-coordinated complex. More recently, an alternative path involving an initial oxoanionic attack on the molybdenum has been studied.[25] However, the calculated activation energies appear to be rather high for an enzymatic reaction. DFT methods have also been used extensively to determine the g-tensors and hyperfine coupling (HFC) constants for transition metal complexes in general[27−29] and molybdenum complexes in particular.[30−32]

In this study we shall first investigate the direct attack of sulfur on the equatorial oxygen of the Mo(VI) center by performing DFT calculations on a model system based on the actual structure of SO. Our findings will further be compared to kinetic studies involving SO[8−10] to establish the plausibility of the calculated energy path. Second, with DFT-based calculations we supplement the experimental ESR investigations carried out to elucidate the electronic structure of the Mo(V). The objective here is to monitor the influence of the co-ligands on the values of the g-tensor components and ^1H hyperfine coupling constants. Of special interest is to determine whether the oxygen-containing ligand in the equatorial plane is hydroxyl or water at high pH conditions.

2. Computational Details and Methods

All calculations were based on DFT as implemented in the ADF program version 2006.01[33] using the Becke-Perdew exchange-correlation functional (BP86)[34−36] and a standard triple-ζ STO basis with one set of polarization functions for all atoms. The 1s electrons of C, N, and O, as well as the 1s−2p electrons of S and 1s−3d electrons of Mo were treated as frozen cores. We represent the protein matrix by a continuum model. The polarizability of the

(6) Wilson, H. L.; Rajagopalan, K. V. *J. Biol. Chem.* **2004**, *279*, 15105.
(7) Thapper, A.; Lorber, C.; Fryxelius, J.; Behrens, A.; Nordlander, E. *J. Inorg. Biochem.* **2000**, *79*, 67.
(8) Chaudhury, P. K.; Das, S. K.; Sarkar, S. *Biochem. J.* **1996**, *319*, 953.
(9) Johnson, J. L.; Rajagopalan, K. V. *J. Clin. Invest.* **1976**, *58*, 543.
(10) Brody, M. S.; Hille, R. *Biochemistry* **1999**, *38*, 6668.
(11) Kisker, C.; Schindelin, H.; Pacheco, A.; Wehbi, W. A.; Garret, R. M.; Rajagopalan, K. V.; Enemark, J. H.; Rees, D. C. *Cell* **1997**, *91*, 973.
(12) Karakas, E.; Wilson, H. L.; Graf, T. N.; Xiang, S.; Jaramillo-Busquets, S.; Rajagopalan, K. V.; Kisker, C. *J. Biol. Chem.* **2005**, *280*, 3506.
(13) Schrader, N.; Fischer, K.; Theis, K.; Mendel, R. R.; Schwarz, G.; Kisker, C. *Structure* **2003**, *11*, 1251.
(14) Enemark, J. H.; Astashkin, A. V.; Raitsimring, A. M. *Dalton Trans.* **2006**, 3501.
(15) Lamy, M. T.; Gutteridge, S.; Bray, R. C. *Biochem. J.* **1980**, *185*, 397.
(16) Astashkin, A. V.; Hood, B. L.; Feng, C.; Hille, R.; Mendel, R. R.; Raitsimring, A. M.; Enemark, H. *Biochemistry* **2005**, *44*, 13274.
(17) Webster, C. E.; Hall, M. B. *J. Am. Chem. Soc.* **2001**, *123*, 5820.
(18) Thapper, A.; Deeth, R. J.; Nordlander, E. *Inorg. Chem.* **2002**, *41*, 6695.
(19) Voityuk, A. A.; Albert, K.; Köstlmeier, S.; Nasluzov, V. A.; Neyman, K. M.; Hof, P.; Huber, R.; Romão, M. J.; Rösch, N. *J. Am. Chem. Soc.* **1997**, *119*, 3159.
(20) Voityuk, A. A.; Albert, K.; Romão, M. J.; Huber, R.; Rösch, N. *Inorg. Chem.* **1998**, *37*, 176.
(21) Zhang, X. H.; Wu, Y. D. *Inorg. Chem.* **2005**, *44*, 1466.
(22) Amano, T.; Ochi, N.; Sato, H.; Sakaki, S. *J. Am. Chem. Soc.* **2007**, *129*, 8131.
(23) Harris, H. H.; George, G. N.; Rajagopalan, K. V. *Inorg. Chem.* **2006**, *45*, 493.
(24) Thapper, A.; Deeth, R. J.; Nordlander, E. *Inorg. Chem.* **1999**, *38*, 1015.
(25) Pal, K.; Chaudhury, P. K.; Sarkar, S. *Chem. Asian J.* **2007**, *2*, 956.
(26) Astashkin, A. V.; Johnson-Winters, K.; Klein, E. L.; Byrne, R. S.; Hille, R.; Raitsimring, A. M.; Enemark, J. H. *J. Am. Chem. Soc.* **2007**, *129*, 14800.
(27) Patchkovskii, S.; Ziegler, T. *J. Chem. Phys.* **1999**, *11*, 5730.
(28) Patchkovskii, S.; Ziegler, T. *J. Am. Chem. Soc.* **2000**, *122*, 3506.
(29) Saladino, A. C.; Larsen, S. C. *Catal. Today* **2005**, *105*, 122.
(30) Fritscher, J.; Hrobárik, P.; Kaupp, M. *J. Phys. Chem. B* **2007**, *111*, 4616.
(31) Fritscher, J.; Hrobárik, P.; Kaupp, M. *Inorg. Chem.* **2007**, *46*, 8146.
(32) Drew, S. C.; Young, C. G.; Hanson, G. R. *Inorg. Chem.* **2007**, *46*, 2388.
(33) (a) Te Velde, G.; Bickelhaupt, F. M.; Baerends, E. J.; van Gisbergen, S.; Guerra, C. F.; Snijders, J. G.; Ziegler, T. *J. Comput. Chem.* **2001**, *22*, 931. (b) www.scm.com.
(34) Becke, A. D. *Phys. Rev. A* **1998**, *38*, 3098.
(35) Perdew, J. P. *Phys. Rev. B* **1986**, *33*, 8822.
(36) Perdew, J. P. *Phys. Rev. B* **1986**, *34*, 7406.

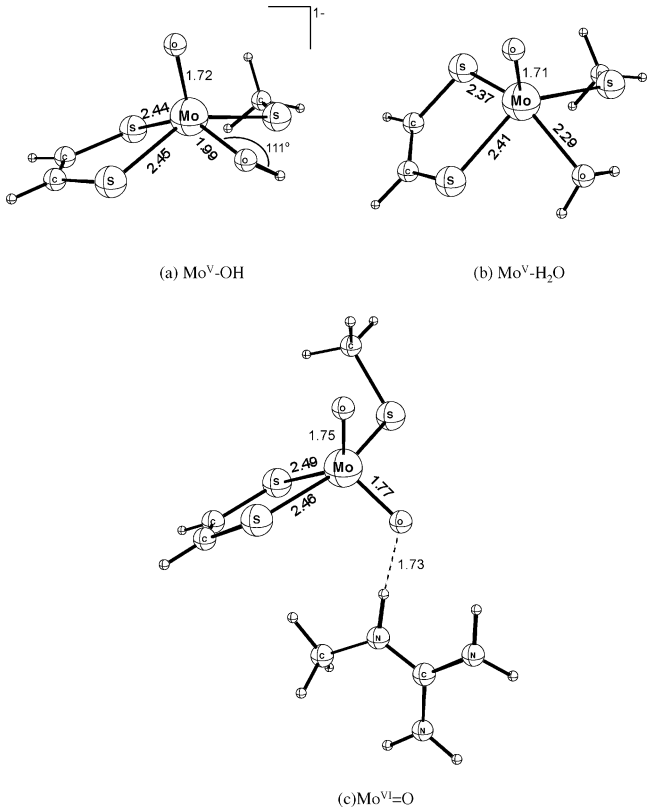

(a) Mo^V-OH (b) Mo^V-H_2O

(c)Mo^{VI}=O

Figure 3. Model systems for sulfite oxidase. (a) In oxidation state Mo(V) with OH^- as the oxygen-containing equatorial ligand. (b) In oxidation state Mo(V) and H_2O as the equatorial ligand. (c) In oxidation state Mo(VI) with an additional methyl guanidinium group.

surrounding protein was included in the mechanistic study by making use of the dielectric continuum model COSMO[37] as implemented in the ADF program for solvation.[38] The solvent excluding surface was used along with a dielectric constant $\epsilon = 5$ in the COSMO calculations.

The starting point of the models used in this study was constructed from the Cartesian coordinates provided by the chicken sulfite oxidase (CSO) X-ray structure, PDB code 1SOX.[11] For all models the pterin cofactor and the Cys 185 were substituted with ene-1,2-dithiolate and methyl thiolate, respectively. Two models were used for Mo(V)−SO with the equatorial oxygen-based ligand being OH^- (Mo^V−OH, (a) in Figure 3), or H_2O (Mo^V−H_2O, (b) in Figure 3). To avoid the approach of two negatively charged species (sulfite and Mo-center) in the oxygen transfer reaction, a neutral system was constructed by adding a methyl guanidinium group (Mo^{VI}=O, (c) in Figure 3). The coordinates of the group were taken as those of Arg 138 from the CSO crystal structure.[11]

The distance between the carbon of the methyl guanidinium group and the molybdenum center was frozen to maintain a distance close to that of the X-ray structure as suggested by Siegbahn.[39] In the actual enzyme the distance is kept by hydrogen bonds and other interactions absent from our model. Approximate transition states were located by performing linear transit calculations in which the remaining degrees of freedom were minimized, while keeping a linear combination of internal coordinates fixed. One possible path for the oxygen transfer reaction involves the attack of the sulfur lone pair from sulfite on the equatorial oxygen attached to the

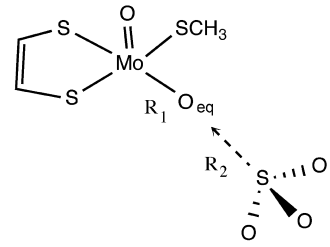

Figure 4. Attack of the SO_3^{2-} ion on the model system Mo^{VI}=O. The guanidinium group is omitted for clarity.

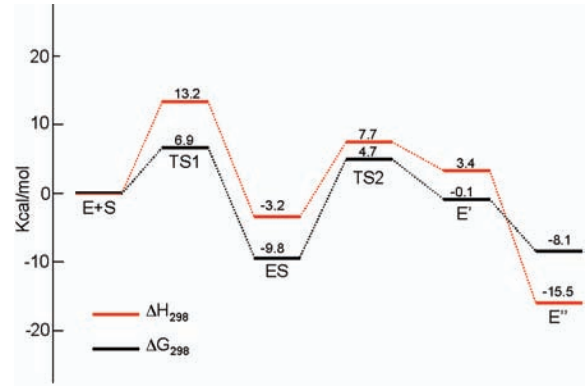

Figure 5. Calculated enthalpy and free energy profiles for the reaction of model Mo^{VI}=O with SO_3^{-2}.

Mo(VI) center as shown in Figure 4. During this attack, the O_{eq}−S distance R_2 decreases while the Mo−O_{eq} distance R_1 increases. We have thus chosen $\Delta R_{12} = R_2 - R_1$ as the reaction coordinate for the oxygen transfer process. Starting from the constrained geometries, all stationary points where then fully optimized[40,41] as minima or transition states. Subsequent gas-phase harmonic frequency analysis calculations were conducted. The reported enthalpies and free energies were computed using the entropy and internal energy values calculated via standard statistical mechanics.

The calculations of g-tensors were performed based on the implementation due to Schreckenbach based on the use of gauge-including atomic orbitals (GIAO) and double perturbation theory.[42] Scalar relativistic effects were included within the quasi-relativistic framework[43] using relativistic frozen core potentials along with the first-order Pauli Hamiltonian. GGA functionals such as BP86 tend to overestimate the covalency of metal−ligand bonds.[44] This overestimation is responsible for the higher values of the g-tensor obtained at the BP86 level.[32] However, studies on molybdenum complexes[30–32] indicate that the overestimation of the g-values is around 2% but the experimental trends, in numerical terms, are well reproduced.

The computation of the ^1H hyperfine coupling constants was carried out with the implementation by van Lenthe et al.[45] within the relativistic zeroth order regular approximation (ZORA)[46] with spin−orbit calculations using the collinear formulation.

(37) Klamt, A.; Schuurmann, G. *J. Chem. Soc., Perkin Trans. 2* **1993**, *5*, 799.
(38) Pye, C. C.; Ziegler, T. *Theor. Chem. Acc.* **1999**, *101*, 396.
(39) Siegbahn, P. E. M.; Borowski, T. *Acc. Chem. Res.* **2006**, *39*, 729.
(40) Versluis, L.; Ziegler, T. *J. Chem. Phys.* **1988**, *88*, 322.
(41) Fan, L.; Ziegler, T. *J. Am. Chem. Soc.* **1992**, *114*, 10890.
(42) Schreckenbach, G.; Ziegler, T. *J. Phys. Chem. A* **1997**, *101*, 3388.
(43) Ziegler, T.; Tschinke, V.; Baerends, E. J.; Snijders, J. G.; Ravenek, W. *J. Phys. Chem.* **1989**, *93*, 3050.
(44) Swann, J.; Westmoreland, D. *Inorg. Chem.* **1997**, *36*, 5348.
(45) van Lenthe, E.; van der Avoird, A.; Wormer, P. E. S. *J. Chem. Phys.* **1998**, *108*, 4783.
(46) van Lenthe, E.; Baerends, E. J.; Snijders, J. G. *J. Chem. Phys.* **1993**, *99*, 4597.

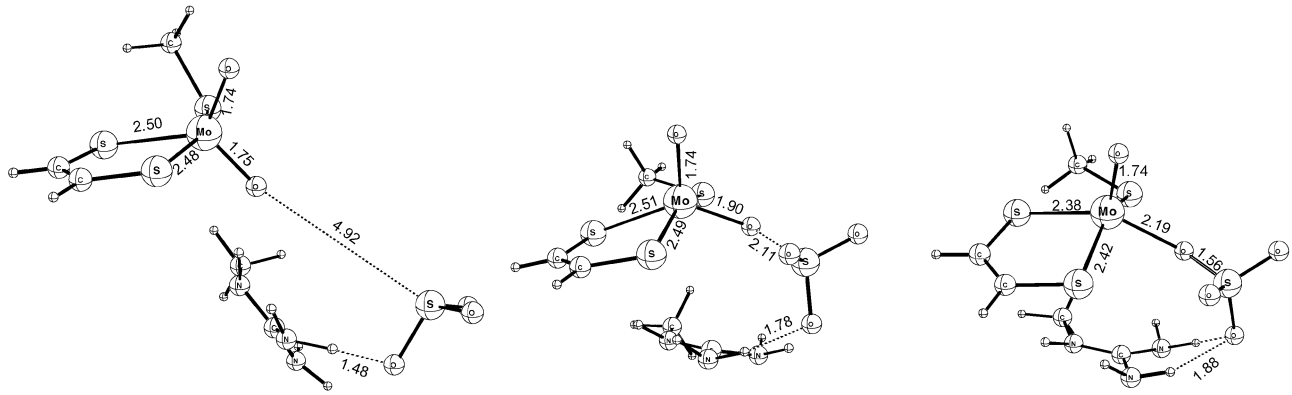

(a) E+S (b) TS1 (c) ES

Figure 6. Geometries of the species involved in the oxidation of sulfite by the Mo(VI)−SO model. (a) Initial structure E+S, (b) first transition state TS1, and (c) intermediate ES. All distances are in angstrom.

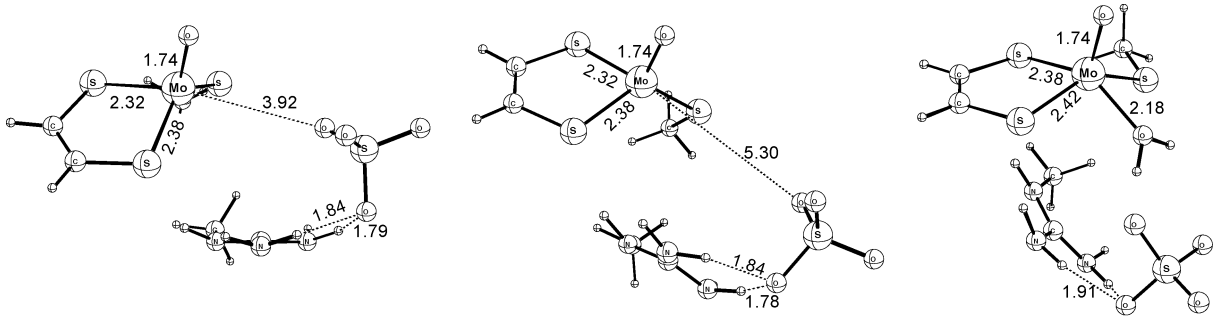

(a) TS2 (b) E' (c) E''

Figure 7. Geometries of the species involved in the release of sulfate and the formation of the Mo(IV)−SO form. (a) Transition state TS2, (b) structure with sulfate dissociated E′, and (c) Mo(IV) with water bound E″. All distances are in angstrom. See also Figure 5.

3. Results and Discussion

Oxidation of Sulfite. In this section we discuss the process by which oxygen is transferred from the Mo(VI) center of sulfite oxidase (SO) to an incoming SO_3^{2-} anion. The result of this step is the formation of SO_4^{2-} and SO in its reduced Mo(IV) oxidation state (step 1, Figure 2). The oxygen transfer reaction has been the subject of both experimental[8–10,12] and theoretical studies.[24,25]

When SO was crystalized in the presence of sulfate, the X-ray structures indicate sulfate adjacent to the molybdenum center.[11,12] They also revealed the interaction of the sulfate with the side chains of the amino acids acting as the substrate binding pocket (Arg-138, Arg-190, Arg-450, Tyr 322, and Trp 204). In our model we shall assume that SO_3^{2-} is attached to the guanidinium group through hydrogen bonding before the oxygen transfer reaction takes place. This starting point is indicated as E+S in the calculated energy profile for the oxygen transfer reaction and in the proposed mechanism given in Figure 5 and Scheme 1, respectively. The optimized structure for E+S is displayed in Figure 6a.

During the oxygen transfer reaction ΔR_{12} decreases as O_{eq} moves from the Mo(VI) center to the sulfur. At the starting point we have $R_1 = 1.75$ Å and $R_2 = 4.92$ Å. Along the path the system reaches a transition state TS1 with an enthalpic barrier of $\Delta H^{\ddagger} = 13.2$ kcal/mol (Figure 5 and Scheme 1). At this transition state R_1 has increased to 1.90 Å whereas R_2 is 2.11 Å, thus indicating some O_{eq}−S bond formation. It is clear that TS1 is an early transition state where the Mo−O_{eq} bond is retained and the O_{eq}−S bond is emerging (see (b) of Figure 6). At the intermediate ES the O_{eq}−S distance is 1.56 Å which is slightly larger than the S−O distance of 1.49 Å in SO_4^{2-}; therefore we can assume that the oxygen has been nearly fully transferred. At the same time the distance R_1 increases to 2.19 Å indicating a partial Mo−O_{eq} bond (see (c) of Figure 6).

To complete the oxidation process, the emerging SO_4^{2-} ion in ES has to be removed from the molybdenum center. This can take place by the transfer of SO_4^{2-} to the guanidinium group and the formation of the adduct E′, followed by the coordination of a water molecule to the Mo(IV) center giving rise to E″ (Scheme 1). In addition, we also studied the associative mechanism in which H_2O and SO_4^{2-} are bound to Mo(IV) at the same time. The corresponding activation energy was found to be approximately 10 kcal/mol larger than for the dissociative mechanism. Thus, in the following we will discuss only the dissociative pathway.

The path from ES to E′ can be described by a further increase in the Mo−O_{eq} distance R_1 in Figure 4. We provide in Figure 5 an energy profile for the sulfate transfer process as a function of the reaction coordinate R_1. The transition state TS2 is associated with an enthalpic barrier of $\Delta H^{\ddagger} = 10.9$ kcal/mol (Figure 5). It follows from the structure of TS2 displayed in Figure 7a that the Mo−O_{eq} bond is broken with a distance of 3.92 Å. At the same time, stabilizing

Table 1. Selected Bond Distances (Å) for the Reduced Form of SO[a]

bond	EXAFS[b]	X-ray[c]	DFT[d]
Mo−O_{ax}	1.72	1.7	1.74
Mo−O_{eq}	2.30	2.3	2.18
Mo−S′ [e]	2.35	2.4	2.42
Mo−S″ [e]	2.35	2.4	2.38

[a] See E″ of Figure 7. [b] Reported in ref 17. [c] From ref 11. [d] Present work. [e] S′ and S″ refer to the dithiolate sulfurs.

Table 2. Kinetic Parameters and Free Energies of Activation and Dissociation for the Reduction of the Molybdenum Center in SO

	k_{red}, s^{-1}	K_d, μM	$\Delta G^{\ddagger}$, kcal/mol	ΔG_d, kcal/mol
Wild type[a]	1871	186	12.3[b]	4.8[c]
Y343F mutant[a]	2084	1634	12.2	3.6
DFT[d]	37	1.36[e]	14.5[g]	9.8[h]
		0.06[f]		

[a] Experimental values from ref 6. [b] Calculated from the experimental rate by means of the transition state theory. [c] Use of the relation $\Delta G_d = -RT \ln K_d$. [d] Present work. [e] Use of $K = (k_{-1} + k_2)/k_1$, see eqs 2 and 3. [f] Use of $K_d = k_{-1}/k_1$. [g] Free energy of activation for ES → E′ in Scheme 1. [h] Free energy of reaction for ES → E + S in Scheme 1.

interactions between the hydrogens of the guanidinium group and the sulfate are created. In the adduct E′ the Mo−O_{eq} bond is completely broken with $R_1 = 5.30$ Å (see (b) of Figure 7). The stabilization of E′ relative to TS2 is 4.3 kcal/mol which we ascribe to the hydrogen bonding between sulfate and guanidinium.

The addition of H_2O finally gives rise to an enthalpic stabilization of $\Delta H_{E'E''} = 18.9$ kcal/mol without any noticeable barrier (Figure 5 and Scheme 1). The structure for the resulting product E″ is shown in Figure 7c; the distance between the molybdenum center and the oxygen of water is 2.18 Å. Additionally, the distances between the dithiolate sulfurs and the metal center are 2.38 and 2.42 Å, respectively, and the axial oxygen−Mo(IV) bond is 1.74 Å. These results correlate very well with the experimental bond lengths determined by X-ray crystallography[11] and high-resolution EXAFS spectroscopy of Mo(IV)−SO[23] as shown in Table 1.

Two sulfate ions per monomer were observed in the crystal structure. One of them was located in the active site and the other around the opening of the active site.[11,12] The second sulfate was identified at 10.6 Å from the molybdenum center and 5.5 Å from Arg-138. The positions of the two sulfates were considered to denote the entry/exit path of the substrate/product to or from the active site.[11] Figure 8 shows the superposition of the X-ray crystal structure of the active site with one bound sulfate and the structure E″. It can be seen that the two structures are similar, especially around the molybdenum center. Although the guanidinium group is not accurately superimposed, the hydrogen-bonding interactions between the guanidinium group and the sulfate are similar in both cases. The excellent correlations with the experimental structure provide confidence in our proposed model of Mo−SO.

Kinetic studies including steady-state and stopped-flow assays with purified enzyme from chicken liver[10] and synthesized SO[6,12] have been carried out to understand the mechanism and the importance of specific residues in the reaction of sulfite oxidase. The experimental results are consistent with a general mechanism in which the first

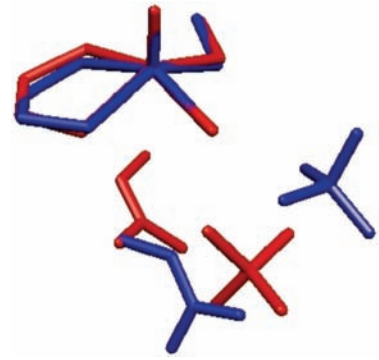

Figure 8. Superposition of the optimized structure E″ (red) and the relevant atoms from the crystal structure (blue). Hydrogens were omitted for clarity.

step is the attack of the sulfite lone pair on one of the Mo(VI)=O units, followed by the generation of a Mo(IV) sulfate adduct and the formation of the sulfate-free reduced Mo(IV) center after the release of a sulfate ion. The process discussed above can be described with the following reaction scheme:

$$A + B \underset{k_{-1}}{\overset{k_1}{\rightleftharpoons}} C \xrightarrow{k_2} D + E \quad (1)$$

where A, B, C, D, and E can be considered as the oxidized enzyme, the sulfite ion, the enzyme-sulfate adduct, the reduced enzyme, and the sulfate ion, respectively. Making use of the steady state condition and assuming the initial concentrations $[B]_0 \gg [A]_0$, a general expression for the apparent first-order rate constant is obtained:[47]

$$k = \frac{k_2 k_1 [B]}{k_{-1} + k_2 + k_1 [B]} \quad (2)$$

Dividing the numerator and the denominator by k_1 we have

$$k = \frac{k_2 [B]}{K + [B]} \quad (3)$$

where K has been defined as

$$K = \frac{k_{-1} + k_2}{k_1} \quad (4)$$

Wilson and Rajagopalan have pointed out that the reduction of the molybdenum center cannot be followed directly by UV−vis spectroscopy in the full protein because of interference from the heme chromophore in the absorption spectra.[6] To avoid this interference, they produced and purified the regions containing only the molybdenum domain and conducted steady-state and stopped-flow kinetic studies using the molybdenum domain. For the stopped-flow experiments the dependence of the experimentally measured rate k_{obs} on the concentration of sulfite (to be denoted as [S]) was found to fit a hyperbolic curve of the form[6]

$$k_{obs} = \frac{k_{red} [S]}{K_d + [S]} \quad (5)$$

where it was assumed that K_d represents the dissociation constant for the intermediate C.[10] A comparison of eqs 3

and 5 leads to the conclusion that k_{red} corresponds to k_2 and $K \approx K_d = k_{-1}/k_1$ only if $k_2 \ll k_{-1}$, that is, the Michaelis−Menten assumption[48] is valid. Table 2 contains the reported rapid kinetic parameters for the reduction of the molybdenum domain at pH = 7.05 and 10 °C.

The calculated energy profile in Figure 5 indicates that the rate-limiting reaction is the formation of the Mo(IV) product (E′). It also shows that all the energy barriers are within the expected values (13−18 kcal/mol) for a typical rate-limiting biochemical reaction.[39] The reaction described by the energy profile is

$$E + S \rightarrow ES \rightarrow E' \rightarrow E'' \quad (6)$$

Considering that the step E′ → E″ proceeds without any noticeable energy barrier, the above reaction can be seen to be in line with the scheme of eq 1 with E + S, ES, and E″ corresponding to the reactants (A and B), the intermediate (C), and the products (D + E), respectively. Thus we can write our particular reaction scheme as

$$E + S \underset{k_{-1}}{\overset{k_1}{\rightleftharpoons}} ES \xrightarrow{k_2} E'' \quad (7)$$

From the experimental rates determined at a single temperature, it is possible to estimate the free energy of activation by means of transition state theory, in which the rate constant k for a reaction is given by

$$k = \frac{k_B T}{h} \exp\left(-\frac{\Delta G^{\ddagger}}{RT}\right)$$

where k_B is the Boltzmann constant, h the Planck constant, R is the gas constant, T the temperature, and $\Delta G^{\ddagger}$ the free energy of activation of the reaction.

Table 2 contains the estimated experimental free energy of activation $\Delta G^{\ddagger}$ for the step ES → E′, and the estimated experimental free energy ΔG_d (assuming that the experimental value is indeed the dissociation constant) for the process ES → E + S. There is reasonable agreement with the experimental data. Our energy profile (Figure 5) does not reproduce the Michaelis−Menten assumption; instead the relationship $k_2 > k_{-1}$ holds. On the basis of our results, it can be proposed that the experimentally fitted values of K_d in eq 5 might not be directly the dissociation constant. In fact, there is some improvement in the agreement with the experimental results when eq 4 is used (Table 2) for K_d rather than k_{-1}/k_1.

It would appear from comparison of our results to experiment that the suggested mode of attack represents a plausible pathway for the oxidation of sulfite by sulfite oxidase. It is likely that the discrepancies between calculated and experimental kinetic parameters are due to entropy contributions from all the amino acids adjacent to the metal center that interact with the substrate and were not considered in our models.

Sarkar et al.[25] have proposed that the enzymatic reaction should proceed by the initial attack of one oxygen of the

Scheme 1. Mechanism Proposed in the Current Work for the Oxidation of SO_3^{2-} by Sulfite Oxidase (Step 1 in Figure 2)[a]

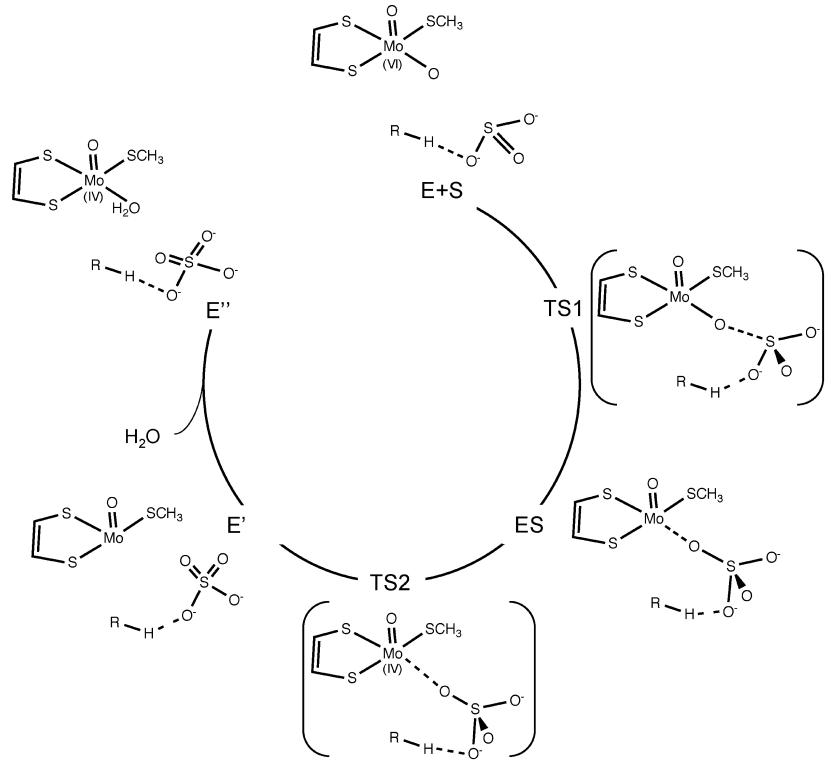

[a] R−H corresponds to a methyl guanidinium group. The corresponding energy profile is given in Figure 5.

substrate to the metal center. Their study considered a model of the molybdenum center similar to our system (Mo^{VI}=O, Figure 6) without the methyl guanidinium and involving HSO_3^- as the substrate instead of SO_3^{2-}. Their resulting mechanism is shown in Scheme 2. They also investigated the attack of the sulfur lone pair of HSO_3^- on the equatorial oxygen of the molybdenum complex. The transition state found (TS* of Scheme 2) has quite similar Mo−O_{eq} and O_{eq}−S bond lengths compared to our TS1 structure. However, Sarkar et al. could not find an intermediate preceding the formation of the Mo(IV) complex (represented by IM* and EP′ in Scheme 2). To introduce an intermediate prior to the formation of IM* (EP′), they modified their mechanism by considering the attack of one oxygen of the HSO_3^- on the metal center.

We were able to locate the intermediate ES due to the inclusion of the methyl guanidinium group. Such a group is absent in the study by Sarkar and co-workers thus preventing the formation of the needed intermediate. Our model emphasizes the importance of the residues next to the active site during the binding/release of the sulfite/sulfate. It can be seen from Figures 6 and 7 that all structures along the pathway show one or two hydrogen bonds between hydrogens of the guanidinium group and the SO_3^{2-} /SO_4^{2-} ions. In the enzyme there are three arginines surrounding the metal center. It is thus reasonable to expect the guanidinium groups of these amino acids to interact with the substrate/product in the same fashion. Therefore, our mechanism shown in Scheme 1 with initial attachment to guanidinium of SO_3^{2-} followed by attack of the sulfur lone pair at the equatorial oxygen seems plausible. It is possible that the initial oxoanionic attack on the metal center shown in Scheme 2 describes better the reaction mechanism of a synthetic analogue such as $[MoO_2(mnt)_2]^{2-}$ (mnt^{2-} = 1,2-dicyanoethylenedithiolate)[8,49] but not necessarily the actual enzyme reaction mechanism. Direct detection of coordinated sulfate in plant SO (At−SO) has been proved experimentally by ESR techniques.[26] However, the structure of that metal center depends upon the method of sample preparation.[16] It is believed that the coordinated sulfate is not rapidly hydrolyzed because the charged funnel in At−SO is narrower compared to the CSO because of the conformation of the aminoacid arginine 450. Depending on its conformation, the accessibility of water molecules to the active site is affected.[16] Our current model does not have a significant spatial restriction for the access of water and can be considered to better describe the CSO case.

Electron Spin Resonance Calculations on Mo(V)−SO Model Systems. In this section we will discuss the results of our ESR calculations on the Mo(V)−SO model systems shown in panels a and b of Figure 3. The paramagnetic and ESR detectable species is formed during step 2 of Figure 2 and has been the subject of several experimental investigations.[14–16,52] Our objective is to compare the calculated ESR parameters such as the g-tensor (**g**) and the isotropic ^{1}H HFC constant (A^{iso}) with experimental data from real Mo(V)−SO systems. Of special interest is the way in which the nature of the equatorial ligands influences **g** and A^{iso}. Additionally we hope by this comparison to shed light on the identity of the oxygen-containing ligand at the equatorial site of the real Mo(V)−SO systems observed at high pH. The different types of SO's studied include enzymes obtained from chicken (CSO),[15] plant (At−SO),[16] and human (HSO).[14] These systems have been further studied at both low (∼6.5) and high (∼10) pH.

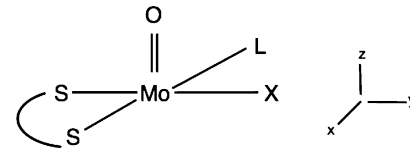

Figure 9. Orientation of the model complexes. L is cysteine in the enzyme and X can be either OH^- or H_2O.

Table 3. Experimental CW-ESR Parameters[a]

form		g_1	g_2	g_3	^{1}H A^{iso}	A_1	A_2	A_3
CSO[15]	hpH[b]	1.9872	1.9641	1.9531	*c*	16[d]	−8	−8
	lpH	2.0037	1.972	1.9658	27.5	24	22	36
HSO[14]	hpH	1.989	1.964	1.954	*c*	*e*		
	lpH	2.0037	1.972	1.9658	26.2	18	20	41
At−SO[16]	hpH	1.989	1.964	1.956	*c*			
	lpH	2.005	1.974	1.963	nd			

[a] Hyperfine coupling constants are in MHz. [b] hpH and lpH represent the high and low pH form, respectively. [c] The A^{iso} has been estimated to be between 0 and 2 MHz.[14] [d] See ref 14. [e] Similar results to those of the anisotropic hyperfine coupling constants of CSO were obtained for At−SO and CSO with slightly different parameters.[14]

For an approximate square pyramidal d^1 complex there will be one principal axial component (g_1), of the g-tensor in the direction along the *z*-axis and two principal equatorial components g_2 and g_3 located in the *xy* plane (Figure 9). The axial component is usually different from the equatorial components; this is also the case for the experimentally observed g-tensors in the real SO systems. The experimental g-tensor values and ^{1}H HFC constants are presented in Table 3. Inspection of Table 3 shows that at high pH all the principal g-values are below the free electron value of g_e = 2.0023; however, this is not the case for the low pH forms of SO where the axial g-values are always slightly greater than g_e.

An analysis of the ESR spectra has established that the equatorial ligand coordinated to molybdenum in the low pH form is OH^-.[15] In the case of the high pH form, two protons seem to be present; however, there was not sufficient evidence to verify whether the ligand is H_2O or OH^- interacting with another OH^- anion from the solvent.[14] The models used for the calculations in our study were named Mo^V−OH (Figure 3a) and Mo^V−H_2O (Figure 3b), and they represent the low pH form and one possible high pH form, respectively. To simulate the other possible high pH form we constructed an additional model, (Mo^V−OH···OH). This model has an equatorial hydroxide ligand interacting with another OH^-, and its optimized geometry is presented in Figure 10.

The calculated ESR parameters are presented in Table 4. There is a good agreement between the experimental ESR data for SO at low pH (lpH) in Table 3 and the calculated ESR parameters for model system Mo^V−OH. This model system is also the only one with a substantial ^{1}H A^{iso} value (35 MHz) that matches the experimental estimate of 26.2−27.5 MHz. Moreover, the model has an axial g_1 value slightly

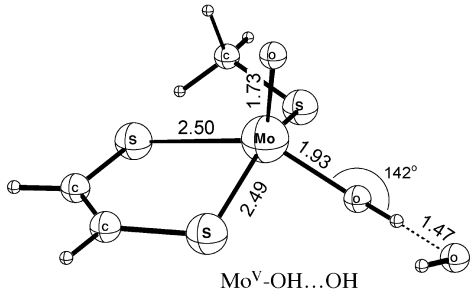

Figure 10. Model for a possible structure of the high pH form of Mo(V)−SO.

above g_e and two equatorial g-values below g_e, which has been found experimentally (Table 3).

ESR experiments on chicken−SO have been carried out at 120 K and 9 GHz with the sample prepared in either H_2O or D_2O.[15] At low pH, the proton hyperfine coupling disappeared when D_2O was used but the measured g-values remained the same, as expected. We have compared the experimental low pH D_2O spectrum with a simulated ESR spectrum for model Mo^V−OH. The software package EasySpin[50] was used. Supporting Information, Figures S2 and S3 show the comparison between the experimental and simulated spectra. It can be seen that our simulated spectrum in Supporting Information, Figure S2 agrees reasonably well with the experimental spectrum in spite of a slight overestimation of the calculated g-tensor values. Supporting Information, Figure S3 displays the comparison between the simulated and experimental spectra from a sample prepared in H_2O where hyperfine coupling is possible. The overestimation of the A-tensor (26.2 MHz experimental vs 35 MHz calculated) in the simulated spectrum gives rise to a larger splitting of the signals.

The experimental ESR data for SO at high pH (hpH) in Table 3 exhibits three principal g-values that are all lower than the free electron value. It has additionally two ^{1}H HFC constant values that are much smaller than those for the low pH SO form. We find that the ESR parameters for the structure in Figure 10 with a OH^- group hydrogen bonded to an equatorial OH^- ligand fit better to the high pH SO experimental data than the parameters for the structure in Figure 3b with H_2O as the equatorial ligand.

It is interesting to note that the model system Mo^V-H_2O, ((b) of Figure 3) has the axial component g_1 much larger than g_e. We shall in the following provide a rationale for the calculated trends in the g_1 values of our three model systems: Mo^V−OH, Mo^V-H_2O, and Mo^V−OH···OH.

The g-tensor, g, can be written as[51]

$$\mathbf{g} = g_e\mathbf{1} + \mathbf{\Delta g} \tag{8}$$

where $\mathbf{\Delta g}$ is the g-shift tensor. The st components of this tensor have the following contributions:

$$\Delta g_{st} = g_e\delta_{st} + \Delta g_{st}^{d} + \Delta g_{st}^{p} \tag{9}$$

where δ_{st} is the Kronecker delta and Δg_{st}^{d} and Δg_{st}^{p} are the diamagnetic and paramagnetic g-shift tensor terms, respectively. The dominant contribution in eq 9 comes from the paramagnetic term. The paramagnetic term can be further broken down into contributions from the magnetic coupling between the singly occupied orbital (SOMO) and the empty orbitals (Δg_{st}^{dd}), the occupied ligand orbitals and the SOMO (Δg_{st}^{Ld}), and between occupied orbitals (Δg_{st}^{oo}):

$$\Delta g_{st}^{p} = \Delta g_{st}^{dd} + \Delta g_{st}^{Ld} + \Delta g_{st}^{oo} \tag{10}$$

It follows from Table 5 that Δg_1^{dd} for all systems is negative[27] whereas both Δg_1^{Ld} and Δg_1^{oo} are positive in all cases.[27]

For the model Mo^V−OH we find that the sum $\Delta g_1^{Ld} + \Delta g_1^{oo}$ is marginally larger than $-\Delta g_1^{dd}$, resulting in a g_1 value slightly larger than g_e. For the model Mo^V-H_2O, $\Delta g_1^{Ld} + \Delta g_1^{oo}$ remains the same as in the previous case whereas $-\Delta g_1^{dd}$ is reduced by a factor of 2 leading to a g_1 value clearly larger than g_e. Finally, with the model Mo^V−OH···OH we note that $-\Delta g_1^{dd}$ remains the same as for Mo^V-H_2O whereas $\Delta g_1^{Ld} + \Delta g_1^{oo}$ is reduced considerably. Consequently the model Mo^V−OH···OH has a g_1 value smaller than g_e. For g_2 and g_3 the negative Δg_1^{dd} contributions are dominant, and we get that both components are smaller than g_e for all three systems.

We can analyze the trends presented in Table 5 in more detail by considering the magnetic coupling between the SOMOs from the three systems and other orbital(s) to produce Δg^{dd} (Figure 11). The SOMO of the low pH model Mo^V−OH is made up mostly of Mo(d_{xy}) and a dithiolate orbital of local b_1 character (the definition of the irreducible representation is possible because the free dithiolate ligand possesses a C_{2v} symmetry). That SOMO will couple with the SOMO+3 made up of Mo($d_{x^2-y^2}$) and a dithiolate a_2 orbital (Table 6 and Figure 11). This coupling has contributions from the interaction between molybdenum d orbitals and between dithiolate b_1 and a_2 orbitals through the magnetic $\hat{M}_z$ operator (Table 7 and Figure 11). The result of this coupling is a large Δg_1^{dd} (Table 6).

Going now to the model Mo^V-H_2O, we note that its SOMO has the same composition as in the model Mo^V−OH. However, it now interacts with the SOMO+4 made up of Mo($d_{x^2-y^2}$) and a dithiolate orbital of b_2 character. In this case, the molybdenum d orbitals can couple magnetically. However, the coupling between the dithiolate b_1 and b_2 orbitals is not possible. The result is that the SOMO/SOMO+4 coupling in the model Mo^V-H_2O is numerically smaller than the SOMO/SOMO+3 coupling in model Mo^V−OH and $-\Delta g_1^{dd}$ is accordingly reduced (Table 6). There is, however, some compensating coupling between the b_1 and the a_2 dithiolate ligand orbitals through the SOMO/SOMO+5 interaction (Figure 11 and Table 6).

Finally, for the second high pH model, Mo^V−OH···OH, we note that the SOMO is lacking a dithiolate component

(47) Strickland, S.; Palmer, G.; Massey, V. *J. Biol. Chem.* **1975**, *250*, 4048.
(48) Voet, D.; Voet, J. G. *Biochemistry*; John Wiley & Sons: New York, 1990; pp 335−337.
(49) Das, S. K.; Chaudhury, P. K.; Biswas, D.; Sarkar, S. *J. Am. Chem. Soc.* **1994**, *116*, 9061.
(50) Stoll, S.; Schweiger, A. *J. Magn. Reson.* **2006**, *178*, 42.
(51) Schreckenbach, G. Relativity and Magnetic Properties. A Density Functional Study; Ph. D. Thesis, University of Calgary, Canada, 1996.
(52) Astashkin, A. V.; Mader, M. L.; Pacheco, A.; Enemark, J. H.; Raitsimring, A. M. *J. Am. Chem. Soc.* **2000**, *122*, 5294.

Table 4. Calculated ESR Parameters[a]

model [b]	equatorial ligand	g_1	g_2	g_3	^{1}H A^{iso}	A_1	A_2	A_3
Mo^V-H_2O	H_2O	2.0270	1.9933	1.9862	10	7	8	15
					3	0	1	8
Mo^V-OH	OH	2.0088	1.9831	1.9793	35	29	28	49
$Mo^V-OH\cdots OH$	OH	1.9943	1.9781	1.9706	2[c]	36	−19	−12
					−3[d]	−2	−4	−3

[a] Hyperfine coupling constants are in MHz. [b] The structures of the models are shown in Figures 3 and 10. [c] Hyperfine coupling of the proton from the hydroxyl ligand. [d] Hyperfine coupling of the proton from the additional hydroxyl group.

Table 5. Major Contributions[a] to the Principal Components of Δg

	g_1			g_2			g_3		
model	Δg^{dd}	Δg^{Ld}	Δg^{oo}	Δg^{dd}	Δg^{Ld}	Δg^{oo}	Δg^{dd}	Δg^{Ld}	Δg^{oo}
Mo^V-OH	−30.90	28.61	8.03	−17.12	1.19	1.15	−23.86	2.38	0.74
Mo^V-H_2O	−15.48	26.58	6.42	−13.37	2.44	1.06	−19.34	4.05	2.27
$Mo^V-OH\cdots OH$	−19.51	3.65	5.38	−22.48	2.64	−0.13	−27.45	1.58	0.20

[a] Contributions in ppt.

Scheme 2. Mechanism Proposed by Sarkar et al.[25] for the Oxidation of HSO_3^- by SO[a]

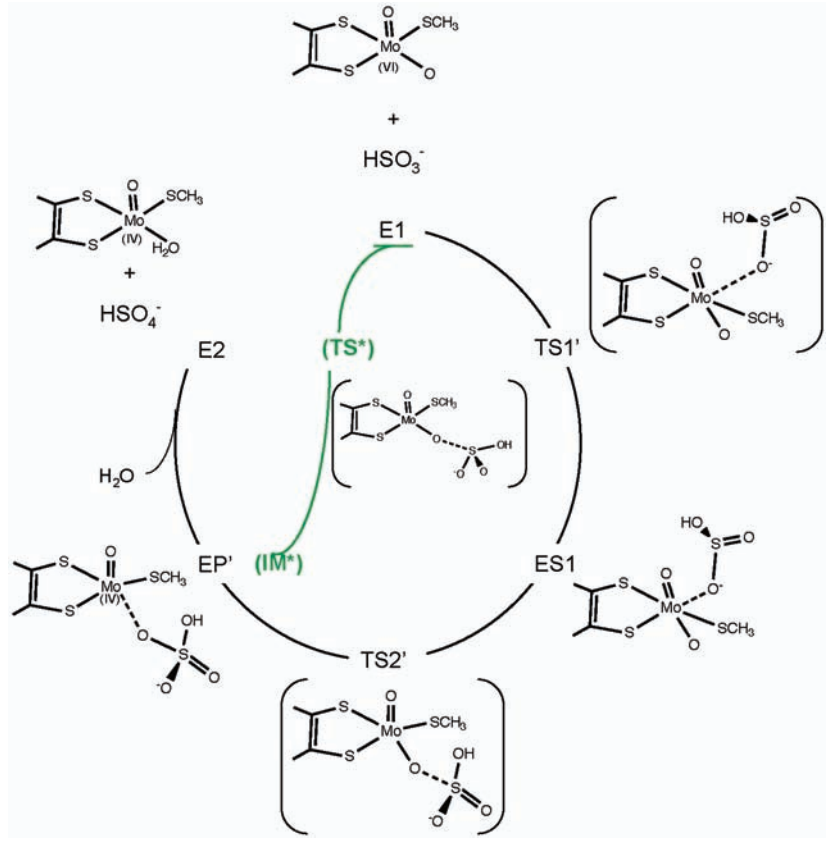

[a] The path shown in green corresponds to the results from their DFT calculations considering the initial attack of the sulfur lone pair of the HSO_3^- ion to the equatorial oxo-ligand. The black path assumes the initial attack of an oxygen of the bisulfite to the metal center.

(Figure 11). As a result its Δg_1^{dd} contribution comes exclusively from the $d_{xy}/d_{x^2-y^2}$ coupling. More importantly, the positive Δg_1^{Ld} contribution is nearly zero because of the lack of coupling between the occupied a_2 dithiolate orbitals and the b_1 component of the SOMO. The overall result is a g_1 component smaller than g_e.

It is worth commenting on the different orientations of the OH^- ligand in the models Mo^V-OH and $Mo^V-OH\cdots OH$. In the first case, the H−Mo−O angle is 111° and the dihedral angle H−O−Mo−S_{cys} is −5°, while in the second structure the respective angles are 142° and 180°. The orientation of the hydroxide ligand in the high-pH model $Mo^V-OH\cdots OH$ allows a Mo−OH π antibonding interaction, thus increasing the energy of the Mo-d_{xy} orbital and consequently avoiding the participation of the a_2 dithiolate ligand in the respective SOMO. The change of orientation of the OH^- ligand in the model $Mo^V-OH\cdots OH$ is the consequence of the interaction with the additional hydroxide. Now, in the case of the low pH model Mo^V-OH, the orientation of the OH^- ligand allows a slight bonding interaction that stabilizes the Mo-d orbital, thus making the subsequent mixing with the dithiolate ligand possible.

We should finally note that the coupling between the dithiolate b_1 orbital in the SOMO and the dithiolate a_2 in

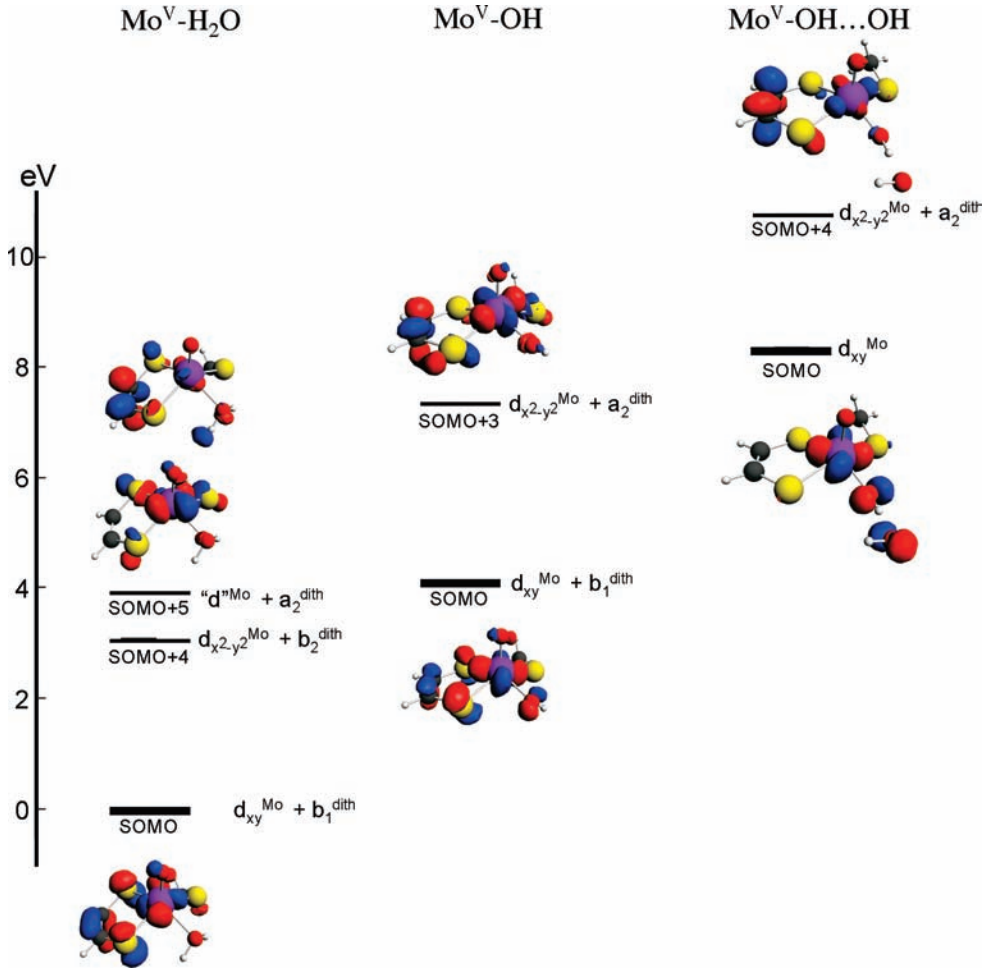

Figure 11. MO diagrams with the principal orbitals that contribute, via magnetic coupling, to the Δg_1^{dd} of models Mo^V−OH and Mo^V−H$_2$O of Figure 3, and Mo^V−OH···OH in Figure 10. The terms b_1^{dith}, b_2^{dith}, and a_2^{dith} refer to the irreducible representation of the dithiolate fragment that contributes to the respective molecular orbital.

Table 6. Major Contributions[a] to the Δg_1^{dd} Component Due to the Coupling of the SOMO with an Empty Orbital

model	equatorial ligand	coupling orbital	Δg_1^{dd}
Mo^V−OH	OH$^-$	SOMO+3	−31.30
Mo^V−H$_2$O	H$_2$O	SOMO+4	−7.79
		SOMO+5	−7.70
Mo^V−OH···OH	OH$^-$···OH$^-$	SOMO+4	−12.34
		SOMO+7	−6.17

[a] Contributions in ppt.

Table 7. Contributions[a] to Δg_1^{dd} in Terms of the Structural Fragment Constituents of the Models Mo^V−OH and Mo^V−H$_2$O

	Mo^V−OH	Mo^V−H$_2$O
Mo	−12.07	−10.47
O_{ax}	−0.77	0.76
O_{eq}	−1.30	−0.05
S_{cys}[b]	−3.33	−0.77
S_{dith}[c]	−13.36	−6.37

[a] Contributions in ppt. [b] Contributions from sulfur on ligand −SCH$_3$. [c] Contributions from sulfur on dithiolate ligand.

the SOMO ± n orbital enters with different signs into Δg_1^{dd} and Δg_1^{Ld}. This is readily understood from perturbation theory as the orbitals with a_2 contribution will have respectively higher (Δg_1^{dd}) and lower (Δg_1^{Ld}) energies than the SOMO.[27]

The indication that the high pH Mo(V) center may be associated with two nearby protons led to the proposition of three different structures to account for this fact.[52] Two of these structures involved a hydroxyl ligand interacting via a hydrogen bond with another hydroxyl or water; the third structure considered H$_2$O as the equatorial ligand. According to the results from our calculations shown in Table 4, we suggest that the most likely structure of the Mo(V) center at high pH contains an equatorial OH$^-$ ligand. A supplementary calculation of ESR parameters on model Mo^V−OH···OH but without the additional hydroxyl group was carried out. The main components of the g-tensor (g_1, g_2, g_3) were found to be (1.9958, 1.9728, 1.9703) and the ^{1}H A^{iso} = 24.6 MHz. In light of these results, we propose that differences in the Mo−OH orientation do have a direct effect on the g-tensor values, as it has been established already for the case of synthetic molybdenum complexes by Fritscher et al.[31] This change in orientation, however, is not enough to explain the ∼30 MHz difference on the isotropic ^{1}H HFC constants (Fritscher et al. only studied the effect on the Mo HFC constant and calculated a difference of ∼ 10 MHz).

The isotropic HFC constant is expected to be a function of the s character of the orbital involved[53] because only electrons in s orbitals have a nonzero probability distribution

(53) Belanzoni, P.; van Lenthe, E.; Baerends, E. J. *J. Chem. Phys.* **2001**, *114*, 4421.

Table 8. Calculated Components of the Proton Hyperfine Tensor[a] and Integrated Electron Valence Spin Density for the s Orbital on H Atom[b]

model	A_1	A_2	A_3	s electron spin density
Mo^V-OH	49	28	28	0.0116
Mo^V-H_2O	6	8	15	0.0099
	0.3	1	9	0.0005
$Mo^V-OH\cdots OH$	-18^c	-12^c	36^c	−0.0019
	-8^d	-2^d	2^d	0.0007
$Mo^V-OH\cdots OH^e$	13	20	41	0.0057

[a] Proton HFC constants in MHz. [b] From Mulliken population analysis; the value shown is the difference of α - β spin. [c] From proton in hydroxyl ligand. [d] From proton in the additional hydroxyl. [e] Calculation of model $Mo^V-OH\cdots OH$ without the additional hydroxyl group.

at the nucleus.[54] Table 8 shows that the interaction between hydroxyl groups in the model $Mo^V-OH\cdots OH$ results in a small negative electron density on the hydrogen from the OH^- ligand (−0.0019) when compared with the density of the same hydrogen not interacting with the additional OH^- group (0.0057), which consequently varies the $A^{iso} = (A_1 + A_2 + A_3)/3$ to give a good qualitative agreement with experimental results. The effects of the conformational differences in the Mo−OH orientation on the ESR parameters of low- and high-pH SO species[14,55] have been noted previously. Our calculations support that the nature of the hydrogen bonding interactions play a main role in the changes of isotropic ^1H HFC constant values going from low to high pH in the actual enzyme. We show that, to obtain a reasonable agreement with the experimental value of the HFC constant at high-pH, the Mo−OH proton should be hydrogen bonded to an oxygen (in our case from the additional OH^-).

George et al.[55] postulated a high-pH structure where the Mo−OH proton was hydrogen-bonded to the tyrosine 343 oxygen. In contrast, the low-pH structure had the proton of the tyrosine−OH group hydrogen-bonded to the oxygen of the Mo−OH. However, ESR studies of the Y343F mutant of human SO also demonstrated that at low-pH the structure might have a coordinated sulfate. At pH = 9.88 the spectrum becomes similar to the low-pH wild type form, and it also contains minor features of the high-pH wild type form.[56] From those results and our calculations, we propose that in the wild type enzyme the conformational differences are due to the interactions between the Mo−OH moiety and the tyrosine 343−OH group. The substitution of tyrosine by phenylalanine in the Y343F mutant might change the surface of the enzyme in such a way that it becomes possible by increasing the pH to widen the opening and facilitate the entrance of water molecules and additional hydroxyl groups to interact with Mo−OH.

4. Concluding Remarks

The use of DFT computational methods allowed us to establish a plausible energy profile for the oxidation of sulfite by SO. It involves the attack of the sulfur lone pair on the equatorial oxo-ligand of the molybdenum center. Our calculated activation energies are in good agreement with the energy parameters derived from various experimental kinetic studies. The importance of the surrounding amino acids to the molybdenum center and their entropic contributions in the oxidation reaction, as well as its importance in the mode of attack of the sulfite, were inferred.

The calculated ESR parameters are in good agreement with the experimental results. The participation of the dithiolate ligand in the SOMO is important for the magnitude of the axial component of the g-shift tensor. The orientation of the H from the OH^- ligand will determine the contribution of the dithiolate ligand to the SOMO. From the calculated parameters, it is suggested that at high pH the two protons detected experimentally belong to an arrangement consisting of the co-ligand OH^- hydrogen bonded to another nearby proton donor (in our case, an additional hydroxide ion) and not coordinated to H_2O. Finally, the difference in the axial component of the g-tensor of the low pH and high pH species is due to the orientation of the hydrogen of the equatorial ligand. For the case of the high pH species, the small isotropic hyperfine coupling constant is due to the hydrogen bond interaction with the nearby proton donor.

Acknowledgment. Some calculations made use of the Western Canada Research Grid computing resources. This work was supported by NSERC. T.Z. thanks the Canadian government for a Canada Research Chair.

Supporting Information Available: Further details are given in Figures S1−S3. This material is available free of charge via the Internet at http://pubs.acs.org.

IC801158T

(54) Wertz, J. E.; Bolton, J. R. *Electron Spin Resonance*; Chapman and Hall: New York, 1996; pp 40−43.
(55) Doonan, C. J.; Wilson, H. L.; Bennett, B.; Prince, R. C.; Rajagopalan, K. V.; George, G. N. *Inorg. Chem.* **2008**, *47*, 2033.
(56) Raitsimring, A. M.; Astashkin, A. V.; Feng, C.; Wilson, H. L.; Rajagopalan, K. V.; Enemark, J. H. *Inorg. Chim. Acta* **2008**, *361*, 941.